Superconducting phases of YH_9 under pressure

Mingyang Du,[1] Zonglun Li,[2] Defang Duan,[2,*] and Tian Cui[1,2,†]

[1]*Institute of High Pressure Physics, School of Physical Science and Technology, Ningbo University, Ningbo, 315211, People's Republic of China*

[2]*State Key Laboratory of Superhard Materials, College of Physics, Jilin University, Changchun 130012, People's Republic of China*

(Received 6 February 2023; accepted 26 October 2023; published 15 November 2023)

Yttrium superhydrides have attracted much attention due to their multiple stoichiometries and excellent superconductivity under high pressure. Especially, YH_9 have a superconducting critical temperature (T_c) of 243 K, which is only second to LaH_{10} among all superconductors. It exhibits a positive pressure dependence of T_c below 200 GPa, contrary to the results of theoretical prediction. In order to explore the origin of T_c at low pressure, we extensively investigated the crystal structures of YH_9 at different pressure, and found a distorted cage structure with a symmetry of *Pnma*. This phase has the lowest enthalpy at pressure below 220 GPa, and its x-ray-diffraction patterns is consistent with experimental data. Most importantly, its pressure dependence of T_c is in line with the experimental results indicating that the low T_c at low pressure mainly comes from the low-symmetry *Pnma* phase. Further calculations show the structural distortion in the *Pnma* phase strongly affects the lattice vibration and electron-phonon coupling induced a positive pressure dependence of T_c. This work uncovers a remarkable correlation between superconductivity and structural distortion, and provides insight into clarifying the dome-shaped superconducting phase diagram (T_c-P) in yttrium hydrides.

DOI: 10.1103/PhysRevB.108.174507

I. INTRODUCTION

As early as in 1935, Winger and Huntington predicted that insulated molecular hydrogen transformed into metal atomic phase under high pressure [1]. And, the metallic hydrogen was predicted to be an ideal high-temperature or even room-temperature superconductor [2]. However, hydrogen metallization was not clearly observed in the experiment even under the extreme high pressure close to 500 GPa [3]. In order to realize hydrogen metallization within the pressure range that diamond-anvil cell can reach, an alternative scheme is proposed—superhydrides.

Introducing other elements into hydrogen produces a "chemical precompression" effect on the hydrogen sublattice, so that hydrogen can exist as a stable atomic phase at a much lower pressure in superhydrides [4]. Inspired by this, many superhydrides have been designed that are expected to exhibit high T_cs [5–10], some of which have been experimentally confirmed. In particular, H_3S and LaH_{10} have high T_cs exceeding 200 K by theoretical predicted and experimental measurement [11–17].

Among these hydrogen-based superconductors, clathrate superhydrides have attracted extensive attention due to their outstanding superconductivity. Predicted by theoretical studies, such structures are common in alkaline earth metals superhydrides and rare-earth metals superhydrides EH_n ($n = 6, 9, 10$), such as binary hydrides CaH_6 [18], MgH_6 [19], $YH_{6,9,10}$ [12,13,20], Sc H_6 [21],and (Tm/Yb/Lu)H_6 [22], and ternary hydrides (Y,Ca)H_6 [23–25], (Mg,Ca)H_6 [26], (Sc,Ca)H_6 [27], (La,Y)H_6 [28], and (Ca/Sc/Y,Yb/Lu)H_6 [29]. These superhydrides contain H_{24}, H_{29}, or H_{32} cages, and metal elements that produce chemical precompression to maintain the stability of the hydrogen cage. After LaH_{10} confirmed the great potential of clathrate superhydrides in high-temperature superconductivity, more clathrate superhydrides were experimentally synthesized, including ThH_9 [30], ThH_{10} [30], YH_9 [31–33], CaH_6 [34,35], YH_6 [36], CeH_9 [37], (La,Y)H_{10} [38], and (La,Ce)$H_{9,10}$ [39,40].

Yttrium superhydrides have been attracting numerous studies due to their excellent properties and multiple stoichiometry. Yttrium superhydrides with the composition YH_3, YH_4, YH_6, and YH_9 have been synthesized. Among them, YH_4 (88 K at 155 GPa [41]), YH_6 (224 K at 166 GPa [36]), YH_9 (243 K at 201 GPa [31], 262 K at 182 GPa [32], and 230 K at 300 GPa [33]) exhibit superconductivity. The theoretical predicted superconductivity of YH_3 (40 K at 17.7 GPa) [42], YH_7 (21.5–43 K at 165 GPa [36]), and YH_{10} (305–326 K at 250 GPa [12]) needs to be further verified experimentally.

YH_9 has the highest T_c among the synthesized yttrium superhydrides, and its T_c is second only to LaH_{10} (250 K at 170 GPa [16] and 260 K at 180 GPa [17]). At first, T_c increases rapidly with the increase of pressure and reaches a maximum value of 243 K at around 200 GPa, and then T_c decreases with the increase of pressure. This dome-shaped superconducting phase diagram (T_c-P) may be associated with the structural distortions and phase transformations. It was found in H_3S [43] and LaH_{10} [44] that their superconductivity was strongly affected by crystal lattice instability toward symmetry-lowering distortions. For YH_9, the $P6_3/mmc$ phase was experimentally confirmed to be the high symmetry and

*duandf@jlu.edu.cn
†cuitian@nbu.edu.cn

high-T_c phase above 200 GPa. For the lower T_c below 200 GPa, it may come from a lower-symmetry structure. In recent years, several structures of YH_9 have been predicted, such as $P6_3/m$ [13], *Cmcm* [13], *P*1 [36], and $F-43m$ [36,45]. But, their stable pressure range, pressure dependence of T_c or x-ray diffraction (XRD) are not in good agreement with experimental results. Therefore, the crystal structure and superconductivity of YH_9 below 200 GPa deserve to be further explored.

In this work, we extensively investigated the high-pressure phases of YH_9, and uncovered a phase with symmetry of *Pnma* between 157 and 220 GPa. The x-ray-diffraction patterns of *Pnma* phase are consistent with previous experimental data. In addition, the T_c of *Pnma* phase increases rapidly with compression, which is also in line with the experimental results. Therefore, the low-T_c phase of YH_9 is most probably from the *Pnma* phase.

II. COMPUTATIONAL DETAILS

The candidate crystal structure of YH_9 was explored by *ab initio* random structure searching technique [46,47] with CAMBRIDGE SERIAL TOTAL ENERGY PACKAGE [48]. Preliminary structural relaxation were performed using the Perdew-Burke-Ernzerhof (PBE) parametrization of the generalized gradient approximation (GGA) [49] for the exchange-correlation functional and on-the-fly generated ultrasoft pseudopotentials (Y 3|2.0|7|8|9|40U:50:41:42 and H 1|0.6|13|15|17|10(qc=8)). Valence electrons were treated as $4s^2$ $4p^6$ $4d^1$ $5s^2$ for Y and $1s^1$ for H.

Final structural relaxation, enthalpies calculations, and all electronic properties were calculated by Vienna *Ab initio* Simulation Program [50], with PBE-GGA. Brillouin-zone (BZ) sampling using Monkhorst-Pack [51] meshed with resolutions of $62\pi \times 0.02\,\text{Å}^{-1}$. The projector-augmented plane-wave potentials (PAW) [52] set cutoff energy of 1000 eV. All parameters were selected to ensure that enthalpy calculations were well converged to be better than 1 meV per atom. Rietveld refinement of the crystal structures were calculated by the GSAS and EXPGUI packages [53].

We used QUANTUM ESPRESSO [54] for electron-phonon coupling (EPC) calculations. PAW-PBE pseudopotentials (Y.pbe-spn-kjpaw_psl.1.0.0.UPF and H.pbe-kjpaw_psl.1.0.0.UPF) from PS Library were used with suitable cutoff energy of 90 Ry. The k-point and q-point meshes in the first BZ are $24 \times 24 \times 24$ and $6 \times 6 \times 6$ for YH_6, $12 \times 12 \times 6$ and $6 \times 6 \times 3$ for *Cmcm* phase, $12 \times 12 \times 12$ and $3 \times 3 \times 3$ for *Pnma* phase, and $12 \times 12 \times 9$ and $6 \times 6 \times 3$ for $P6_3/mmc$ phase. T_c of these structures are calculated by the Allen-Dynes-modified McMillan equation with correction factor s [55,56] and self-consistent iteration solution of the Eliashberg equation (scE) [57].

III. RESULTS AND DISCUSSION

Ab initio random structure searches were focused on YH_9 with 1 to 4 formula units under pressure of 100–300 GPa. A stable phase with symmetry of *Pnma* was uncovered in the pressure range considered. Their crystal structures are listed in Table S1 of the Supplemental Material [58].

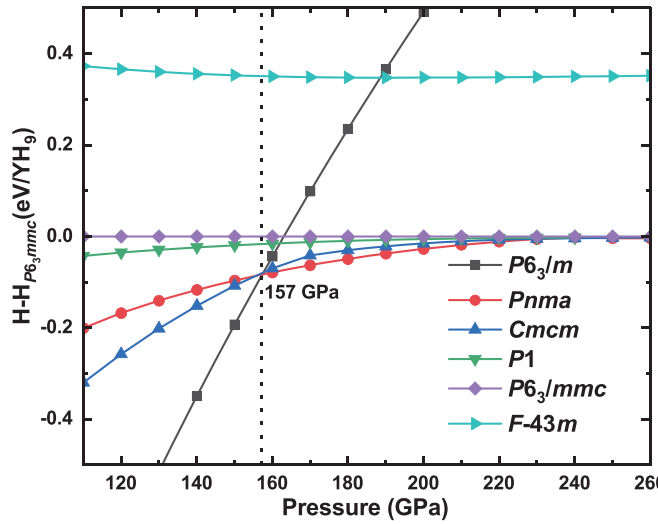

FIG. 1. Calculated enthalpies of various phases relative to $P6_3/mmc$ phase as function of pressure.

Figure 1 shows the pressure dependence of enthalpies for phases that are found in this work and previous studies. $P6_3/m$ phase is the most stable phase at pressure below 157 GPa, which is a layered structure, and each layer is composed of Y atom and H_3 molecular units [see Fig. 2(a)]. The enthalpy of the *Pnma* phase is lower than that of the $P6_3/m$ phase at the pressure above 157 GPa, and *Pnma* phase becomes the most stable one. Finally, the highly symmetric $P6_3/mmc$ structure proposed by Peng *et al.* [13] becomes favorable above 220 GPa. The $P6_3/mmc$ phase is a kind of clathrate structure with H_{29} cage, which widely exists in rare-earth metal superhydrides at high pressure. In this structure, H atoms are bonded covalently to form hydrogen cage, and rare-earth metal atoms are located in the centers of the hydrogen cages [see Fig. 2(b)]. The crystal structures of *Pnma*, *Cmcm,* and *P*1 phases are all similar to that of $P6_3/mmc$ phase [see Figs. 2(c)–2(e)]. In terms of space groups, *Cmcm* is a subset of group

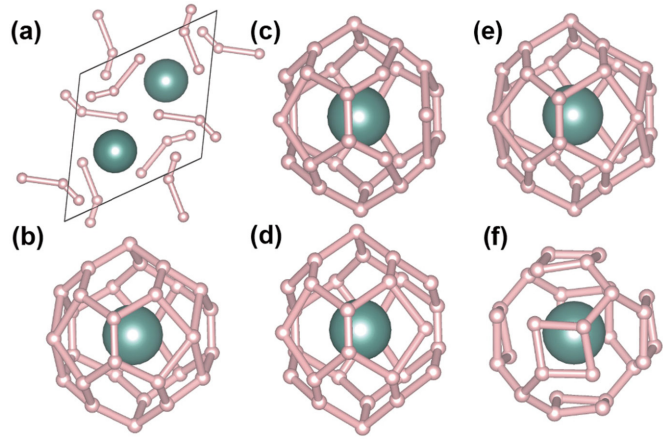

FIG. 2. Layered structures of (a) $P6_3/m$, and clathrate structures of (b) $P6_3/mmc$, (c) *Pnma*, (d) *Cmcm*, (e) *P*1, and (f) $F-43m$.

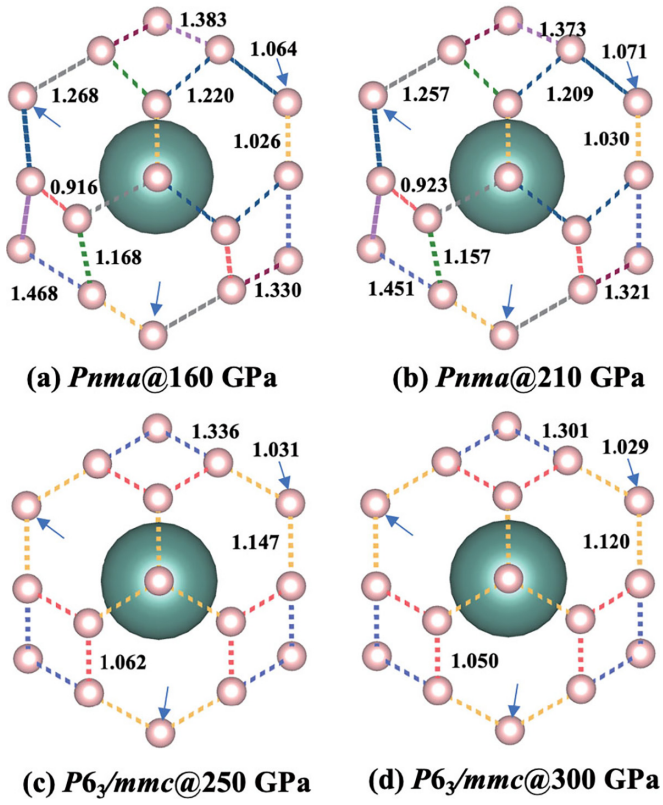

FIG. 3. H–H distances (Å) in H_{29} cage of *Pnma* phase at (a) 160 GPa and (b) 210 GPa; $P6_3/mmc$ phase at (c) 250 GPa and (d) 300 GPa. The H–H bond with same color in same structure have same length. Three H atoms pointed out by arrow have H–H bonds perpendicular to plane, whose lengths are marked on arrows at upper right corner.

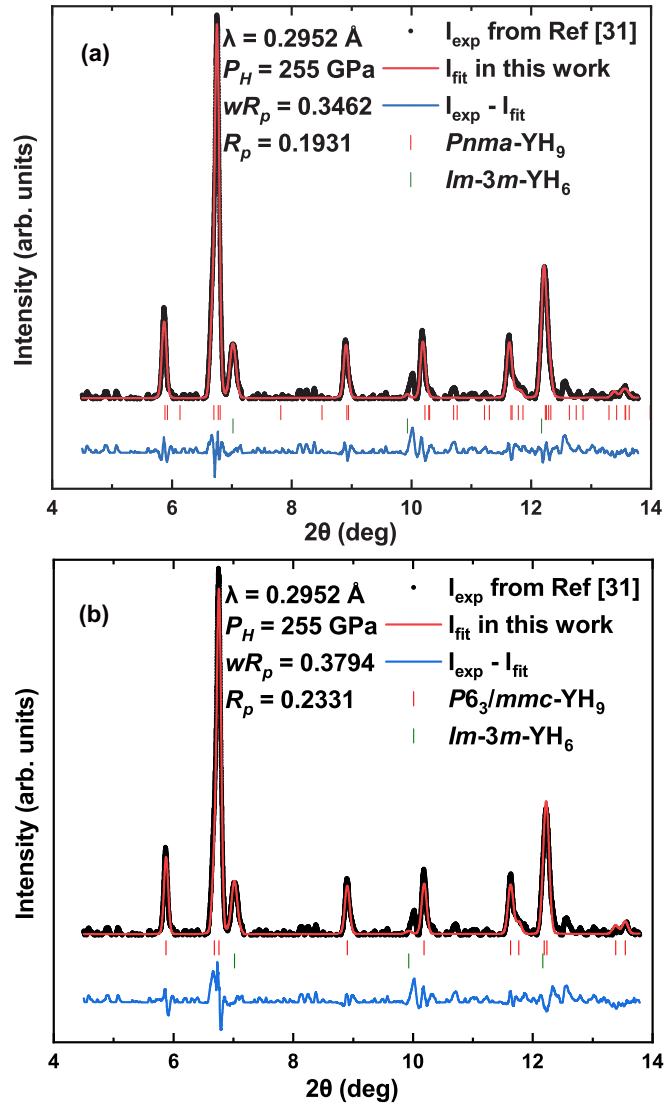

FIG. 4. X-ray-diffraction patterns of synthesized yttrium hydrides compared with simulated diffraction peaks of (a) $Pnma{-}YH_9 + Im{-}3m{-}YH_6$ and (b) $P6_3/mmc{-}YH_9 + Im{-}3m{-}YH_6$. Black circles, red curves, and blue curves correspond to experimental data provided by Kong *et al.* [31], Rietveld refinement fits, and differences in this work, respectively.

$P6_3/mmc$, and *Pnma* is a subset of group *Cmcm*. The *P-V* curve of *Cmcm* phase was consistent with *Pnma* phase above 170 GPa and there was no drastic change in volume during the phase transition (see Fig. S6 [58]). Therefore, *Pnma* can be linked with *Cmcm* phase by second-order phase transition and structural distortions. With the increase of pressure, the degree of distortion is narrowing, and they transform into the $P6_3/mmc$ phase above 220 GPa. After considering the zero-point energy, *Pnma* phase is still thermodynamic stability above 157 GPa and $P6_3/mmc$ can be thermodynamic stable above 197 GPa (see Fig S1 [58]). The $F-43m$ is a metastable phase with high enthalpy. The $F-43m$ phase contains H_{28} cage, equivalent to a twisted H_{32} cage (such as LaH_{10} [12]) missing four H atoms [see Fig. 2(f)], and similar structure exists in PrH_9 [59].

To determine the dynamic stability of $P6_3/m$, *Pnma*, *Cmcm*, and $P6_3/mmc$ phases, we calculated their phonon spectra at different pressures. For $P6_3/m$ phase, no imaginary frequency mode at 140 and 150 GPa (see Fig S2 [58]) indicated its dynamically stability in this pressure range. *Cmcm* phase can be dynamically stable between 100 and 150 GPa (see Fig S3 [58]), while *Pnma* phase is dynamically stable in the pressure range of 160–210 GPa This is consistent with the thermodynamically stability that *Pnma* phase has lower enthalpy than *Cmcm* above 157 GPa. As the case of $P6_3/mmc$ phase, it can be dynamically stable above 250 GPa. When the pressure is below 250 GPa, imaginary modes will occur along *G-M* and *G-K*, as shown in Fig S5 [58]. It indicates that the phase transition from $P6_3/mmc$ to *Pnma* is due to the symmetry breaking caused by phonon softening. At 210–250 GPa, all known YH_9 phases are unstable. There would be an uncovered stable structure with more atoms, or the anharmonic effects may cause the $P6_3/mmc$ phase to dynamically stabilize down to 210–250 GPa. However, the detailed study requires a rather large amount of computation, which we will probably carry out in future work.

To compare the structural distortion of H_{29} cage in *Pnma* phase with that in $P6_3/mmc$ phase, their detailed configurations of H_{29} cage at different pressures and the corresponding H-H distances are shown in Fig. 3. *Pnma* phase has nine

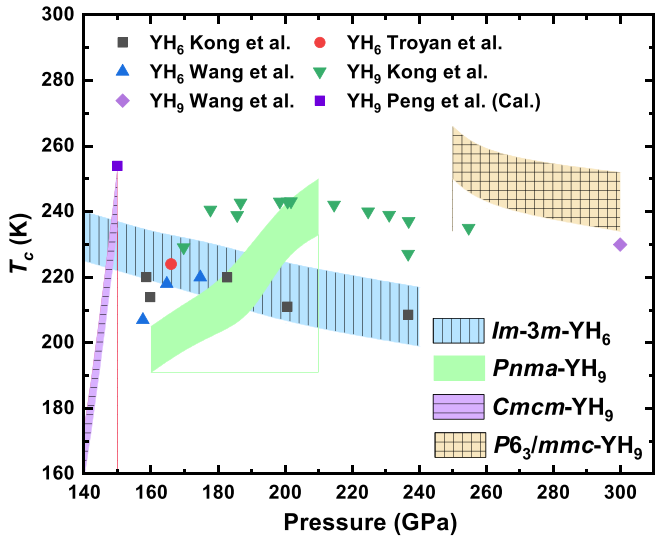

FIG. 5. Pressure dependence of T_c for $Im-3m$ phase of YH_6, and *Cmcm*, *Pnma*, and $P6_3/mmc$ phases of YH_9. Stained areas represent results of theoretical prediction, and points represent results of previous theoretical prediction [13] and experimental measurement [31,33,36].

kinds of H–H bonds with different lengths that induce the distortion of the H_{29} cages. As the pressure increases from 160 to 210 GPa, all H–H bonds longer than 1.1 Å shorten, while three kinds of H–H bonds shorter than 1.1 Å (marked with red, yellow, and arrow) stretch [see Figs. 3(a) and 3(b)]. $P6_3/mmc$ phase has only four kinds of H–H bonds and all H–H bonds shorten with increasing pressure [see Figs. 3(c) and 3(d)].

We furthermore calculated the Bader charge of *Pnma* and $P6_3/mmc$ phases at different pressures (see Table S2). In the *Pnma* phase at 160 GPa, the charges accepted per H atom varies from 0.1 to 0.35 e. Five different kinds of H atoms can be distinguished according to the charges obtained. As the pressure rises to 210 GPa, the electrons gained by H atoms more than 0.14 e decrease, while that less than 0.14 e increase. $P6_3/mmc$ phase with the high symmetry has three kinds of H atoms and the electrons gained by H atoms reduce with the increase of pressure. The electrons obtained by H atoms can fill the antibonding state of the H–H bonds, which affects the length of H–H bond. Therefore, we can see that the essential reason why the H–H bond length converges with the increase of pressure is that the pressure makes the charge more evenly distributed, which is actually conducive to superconductivity. For $P6_3/mmc$ phase, the electrons accepted per H atom donated by the Y metal is basically evenly distributed. However, as the pressure increases, the total charges transferred by the Y atom decreases, which leads to a decrease in charges gained by all H atoms, thus leading to the shortening of H–H bonds.

Due to the lower enthalpy and similar structure, we consider that the previously synthesized yttrium hydrides also contain *Pnma* phase, so we calculated the XRD patterns of *Pnma* phase and compared it with the experimental data measured by Kong *et al.* [31] (see Fig. 4). The fitting result shows that *Pnma* phase [$R_p = 19.31\%$ and $wR_p = 34.62\%$;

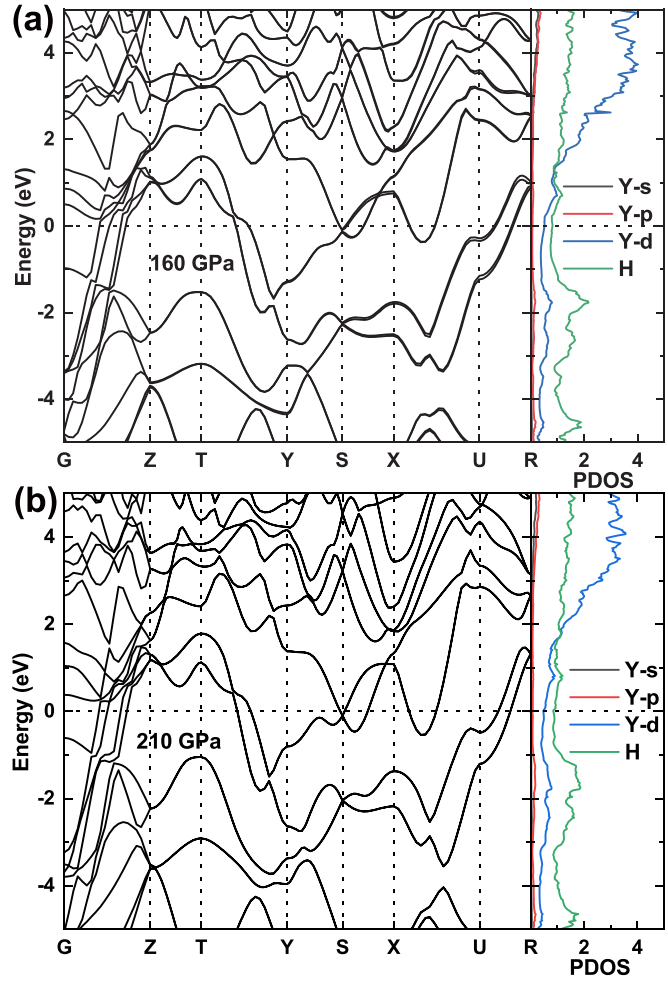

FIG. 6. Calculated electronic band structures and projected density of states (PDOS) for *Pnma* phase at (a) 160 GPa and (b) 210 GPa.

see Fig. 4(a)] is more consistent with experimentally synthesized yttrium hydrides than $P6_3/mmc$ phase [$R_p = 23.31\%$ and $wR_p = 37.94\%$; see Fig. 4(b)]. This indicates that the *Pnma* phase is very likely to be the YH_9 phase with low symmetry and low T_c we are looking for.

Figure 5 shows the pressure dependence of critical temperature for $Im-3m$ phase of YH_6, and *Cmcm*, *Pnma*, and $P6_3/mmc$ phases of YH_9. The stained areas represent the results estimated through the Eliashberg equation with Coulomb pseudopotential of $\mu^* = 0.1$ and 0.13. The points represent the result of theoretical prediction by Peng *et al.* [13], experimental observations by Kong *et al.* [31], Troyan *et al.* [36], and Wang *et al.* [33]. Our prediction of YH_6 (blue area) is in good agreement with the experimental observation (black points), which indicates that our calculations are accurate for yttrium hydrides. It can be seen from Fig. 5 that the estimated T_cs of *Cmcm* phase are 152–167 K at 140 GPa, and 235–253 K at 150 GPa, which deviate from experimental data. Note that the estimated T_cs of *Pnma* increase with increasing pressure, from 191–205 K at 160 GPa to 233–250 K at 210 GPa, which is in line with the pressure dependence of T_c in experiments. Above 250 GPa, the predicted T_cs of $P6_3/mmc$ phase, decrease

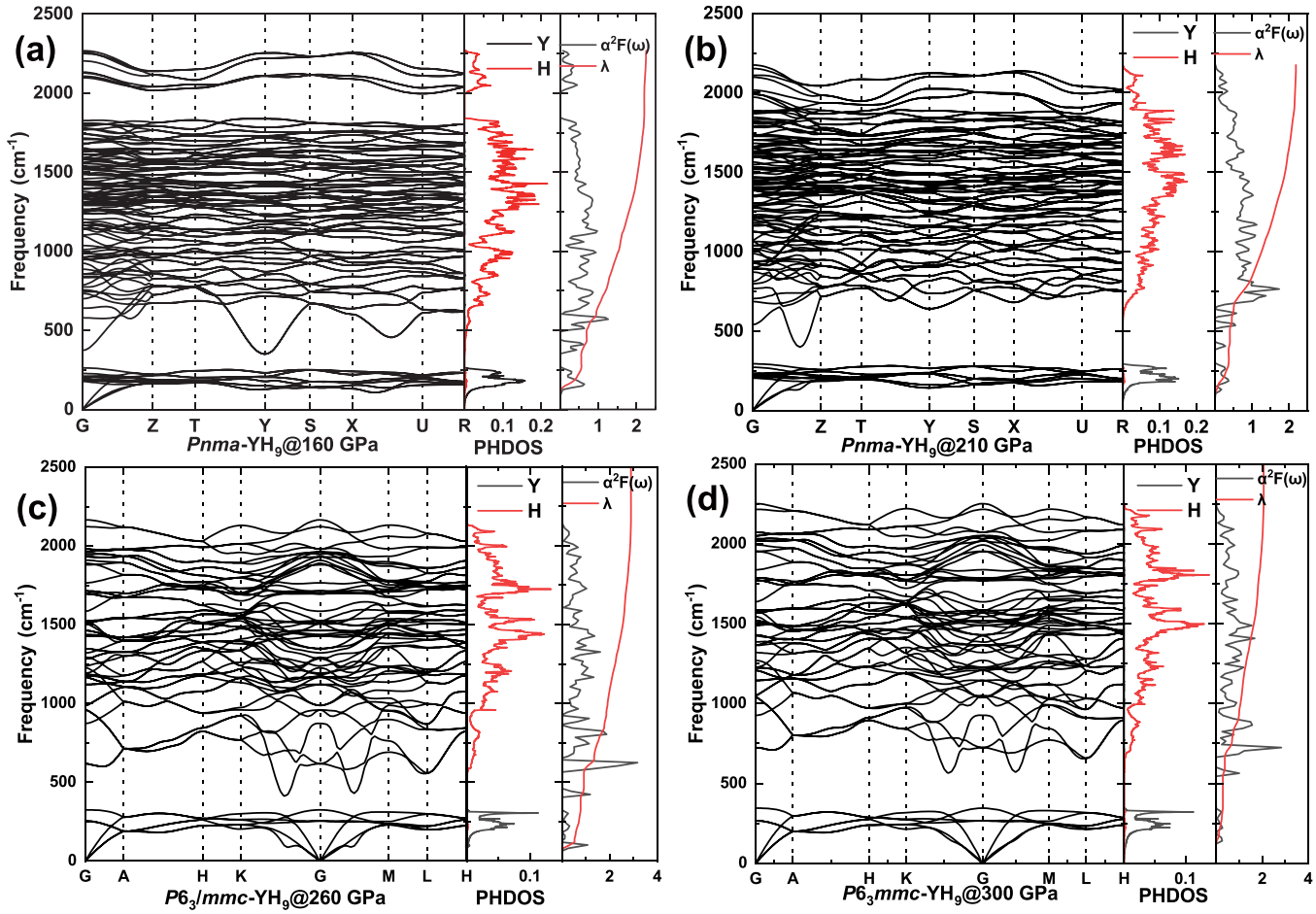

FIG. 7. Calculated phonon dispersion curves, PHDOS, electron-phonon coupling (EPC) parameter λ, and Eliashberg spectral function $\alpha^2F(\omega)$ of electronic band structures and projected density of states for *Pnma* phase at (a) 160 GPa and (b) 210 GPa, and $P6_3/mmc$ phase at (c) 260 GPa and (d) 300 GPa.

with increasing pressure (250–266 K at 250 GPa to 234–252 K at 300 GPa), which is consistent with the experimental trend.

Subsequently, we calculated the electronic band structures and projected density of states (PDOS) to understand the effect of pressure on the electronic structure for the *Pnma* phase. As shown in Fig. 6, contributions from H *s* orbitals and Y *d* orbitals dominate the DOS at the Fermi level. At 160 GPa, the energy band structure of the *Pnma* phase has many split energy bands along the *X*-*U*-*R* path [see Fig. 6(a)]. When the pressure rises to 210 GPa, these bands degenerate [see Fig. 6(b)]. It may be related to the diminishing of H_{29} cage distortion in *Pnma* phase with the increase of pressure.

Although *Pnma* and $P6_3/mmc$ phases have similar structure, their pressure dependence of T_c is different: with compression the T_c of *Pnma* phase increases rapidly while the T_c of $P6_3/mmc$ phase decreases. To further understand the different pressure dependence of T_c, we calculated the phonon dispersion curves and Eliashberg spectral function $\alpha^2F(\omega)$ of *Pnma* and $P6_3/mmc$ phases at different pressures, as shown in Fig. 7. For *Pnma* phase in Figs. 7(a) and 7(b), it can be seen from phonon dispersion curves (PHDOS) that the low-frequency phonon modes (below 250 cm^{-1}) are mainly from Y atom, medium-frequency phonon modes (300–1800 cm^{-1}) are mainly from bending modes of H atom, and high-frequency phonon modes (above 2000 cm^{-1}) are entirely from H_2 molecular units. As we discussed in Fig. 3, compression will promote a more even distribution of charges, thus making short bonds longer and long bonds shorter. With increasing pressure, short H–H bonds in H_2 molecular units stretch and high-frequency vibrations diminish, while long H–H bonds contract and medium-frequency vibration enhance [see Fig. 7(b)], leading to the increase of average phonon frequency. Logarithmic average phonon frequency $\omega_{\log}$ of the *Pnma* phase increases from 890 K at 160 GPa to 1153 K at 210 GPa (see Table S3). We know that the increase of superconducting transition temperature mainly comes from the enhancement of electron-phonon coupling and the increase of average phonon frequency. For the *Pnma* phase, the λ change a little with increased pressure, which is 2.26 at 160 GPa and 2.19 at 210 GPa. Therefore, the increase of $\omega_{\log}$ makes the T_c of *Pnma* phase increase rapidly from 191–205 to 233–250 K in the pressure range of 160–210 GPa.

For $P6_3/mmc$- phase, it exhibits prominent phonon "softening" at 260 GPa, and the softening becomes weaker with the increase of pressure, which leads to the weakening of electron-phonon coupling. The λ is 2.90 at 260 GPa and 2.06

at 300 GPa. Although the ω_{log} increases with compression from 790 K at 260 GPa to 1255 K at 300 GPa (see Table S3), it cannot counteract the influence of electron-phonon coupling weakening. Therefore, $P6_3/mmc$ phase shows a decreasing trend of T_c with the increase of pressure, from 250–266 to 234–252 K in the pressure range of 250–300 GPa.

IV. CONCLUSIONS

In summary, we have systematically explored the crystal structures of YH_9 up to 300 GPa by random structure searching method, and found a lowly symmetric *Pnma* phase with distorted H_{29} cage. This phase is predicted to be stable between 160 and 210 GPa, and its XRD and pressure dependence of T_c are consistent with the experimental results. Further calculations show that the charge distribution in *Pnma* phase tends to be average with increasing pressure, which weakens the distortion of H_{29} cage, and finally exhibit a positive pressure dependence of T_c. This phenomenon has been experimentally established in LaH_{10} and H_3S. Our findings not only provide a theoretical support to the experimental observations, but also shed light on the correlation between superconductivity and structural distortion in YH_9.

ACKNOWLEDGMENTS

We are grateful to Vasily S. Minkov and Mikhail I. Erements who provide experimental data in Fig. 4. We are also grateful to Feng Peng who provide crystal structure of *Cmcm*-YH_9. This work was supported by the National Natural Science Foundation of China (Grants No. 52072188, No. 12122405, and No. 12274169), Program for Science and Technology Innovation Team in Zhejiang (Grant No. 2021R01004). Parts of calculations were performed in the High Performance Computing Center (HPCC) of Jilin University and TianHe-1(A) at the National Supercomputer Center in Tianjin.

The authors declare no competing financial interest.

[1] E. Wigner and H. B. Huntington, On the possibility of a metallic modification of hydrogen, J. Chem. Phys. **3**, 764 (1935).

[2] N. W. Ashcroft, Metallic hydrogen: A high-temperature superconductor? Phys. Rev. Lett. **21**, 1748 (1968).

[3] P. Loubeyre, F. Occelli, and P. Dumas, Synchrotron infrared spectroscopic evidence of the probable transition to metal hydrogen, Nature (London) **577**, 631 (2020).

[4] N. W. Ashcroft, Hydrogen dominant metallic alloys: High temperature superconductors? Phys. Rev. Lett. **92**, 187002 (2004).

[5] D. F. Duan, Y. X. Liu, Y. B. Ma, Z. Shao, B. B. Liu, and T. Cui, Structure and superconductivity of hydrides at high pressures, Natl. Sci. Rev. **4**, 121 (2017).

[6] M. Du, W. Zhao, T. Cui, and D. Duan, Compressed superhydrides: The road to room temperature superconductivity, J. Phys.: Condens. Matter **34**, 173001 (2022).

[7] J. K. Jiayu Ma, W. Cui, J. Chen, K. Gao, J. Hao, J. Shi, and Y. Li, Metal-element-incorporation induced superconducting hydrogen clathrate structure at high pressure, Chin. Phys. Lett. **38**, 027401 (2021).

[8] Q. F. Yiding Liu, J. Yang, L. Wang, W. Zhang, and G. Yao, Predicted high-temperature superconductivity in rare earth hydride ErH_2 at moderate pressure, Chin. Phys. Lett. **39**, 127403 (2022).

[9] T. Huang *et al.*, Metallic aluminum suboxides with ultrahigh electrical conductivity at high pressure, Research **2022**, 9798758 (2022).

[10] X. Yi, Z. Liao, J. You, B. Gu, and G. Su, Superconducting, topological, and transport properties of kagome metals $CsTi_3Bi_5$ and $RbTi_3Bi_5$, Research **6**, 0238 (2023).

[11] D. F. Duan *et al.*, Pressure-induced metallization of dense $(H_2S)_2H_2$ with high-T_c superconductivity, Sci. Rep. **4**, 6968 (2014).

[12] H. Y. Liu, Naumov II, R. Hoffmann, N. W. Ashcroft, and R. J. Hemley, Potential high-T_c superconducting lanthanum and yttrium hydrides at high pressure, Proc. Natl. Acad. Sci. USA **114**, 6990 (2017).

[13] F. Peng, Y. Sun, C. J. Pickard, R. J. Needs, Q. Wu, and Y. M. Ma, Hydrogen clathrate structures in rare earth hydrides at high pressures: Possible route to room-temperature superconductivity, Phys. Rev. Lett. **119**, 107001 (2017).

[14] A. P. Drozdov, M. I. Eremets, I. A. Troyan, V. Ksenofontov, and S. I. Shylin, Conventional superconductivity at 203 kelvin at high pressures in the sulfur hydride system, Nature (London) **525**, 73 (2015).

[15] M. Einaga, M. Sakata, T. Ishikawa, K. Shimizu, M. I. Eremets, A. P. Drozdov, I. A. Troyan, N. Hirao, and Y. Ohishi, Crystal structure of the superconducting phase of sulfur hydride, Nat. Phys. **12**, 835 (2016).

[16] A. P. Drozdov *et al.*, Superconductivity at 250 K in lanthanum hydride under high pressures, Nature (London) **569**, 528 (2019).

[17] M. Somayazulu, M. Ahart, A. K. Mishra, Z. M. Geballe, M. Baldini, Y. Meng, V. V. Struzhkin, and R. J. Hemley, Evidence for superconductivity above 260 K in lanthanum superhydride at megabar pressures, Phys. Rev. Lett. **122**, 027001 (2019).

[18] H. Wang, J. S. Tse, K. Tanaka, T. Iitaka, and Y. Ma, Superconductive sodalite-like clathrate calcium hydride at high pressures, Proc. Natl. Acad. Sci. USA **109**, 6463 (2012).

[19] X. Feng, J. Zhang, G. Gao, H. Liu, and H. Wang, Compressed sodalite-like MgH_6 as a potential high-temperature superconductor, RSC Adv. **5**, 59292 (2015).

[20] Y. Li, J. Hao, H. Liu, J. S. Tse, Y. Wang, and Y. Ma, Pressure-stabilized superconductive yttrium hydrides, Sci. Rep. **5**, 9948 (2015).

[21] K. Abe, Hydrogen-rich scandium compounds at high pressures, Phys. Rev. B **96**, 144108 (2017).

[22] H. Song, Z. Zhang, T. Cui, C. J. Pickard, V. Z. Kresin, and D. Duan, High T_c superconductivity in heavy rare earth hydrides, Chin. Phys. Lett. **38**, 107401 (2021).

[23] H. Xie *et al.*, High-temperature superconductivity in ternary clathrate $YCaH_{12}$ under high pressures, J. Phys.: Condens. Matter **31**, 245404 (2019).

[24] X. Liang, A. Bergara, L. Wang, B. Wen, Z. Zhao, X.-F. Zhou, J. He, G. Gao, and Y. Tian, Potential high-T_c superconductivity in $CaYH_{12}$ under pressure, Phys. Rev. B **99**, 100505(R) (2019).

[25] W. Zhao, D. Duan, M. Du, X. Yao, Z. Huo, Q. Jiang, and T. Cui, Pressure-induced high-T_c superconductivity in the ternary clathrate system Y-Ca-H, Phys. Rev. B **106**, 014521 (2022).

[26] W. Sukmas, P. Tsuppayakorn-aek, U. Pinsook, and T. Bovornratanaraks, Near-room-temperature superconductivity of Mg/Ca substituted metal hexahydride under pressure, J. Alloy. Compd. **849**, 156434 (2020).

[27] L.-T. Shi, Y.-K. Wei, A. K. Liang, R. Turnbull, C. Cheng, X.-R. Chen, and G.-F. Ji, Prediction of pressure-induced superconductivity in the novel ternary system $ScCaH_{2n}$ (n = 1–6), J. Mater. Chem. C **9**, 7284 (2021).

[28] P. Song, Z. Hou, P. B. d. Castro, K. Nakano, K. Hongo, Y. Takano, and R. Maezono, High-T_c superconducting hydrides formed by LaH_{24} and YH_{24} cage structures as basic blocks, Chem. Mater. **33**, 9501 (2021).

[29] M. Du, H. Song, Z. Zhang, D. Duan, and T. Cui, Room-temperature superconductivity in Yb/Lu substituted clathrate hexahydrides under moderate pressure, Research **2022**, 9784309 (2022).

[30] D. V. Semenok *et al.*, Superconductivity at 161 K in thorium hydride ThH_{10}: Synthesis and properties, Mater. Today **33**, 36 (2020).

[31] P. Kong *et al.*, Superconductivity up to 243 K in the yttrium-hydrogen system under high pressure, Nat. Commun. **12**, 5075 (2021).

[32] E. Snider, N. Dasenbrock-Gammon, R. McBride, X. Wang, N. Meyers, K. V. Lawler, E. Zurek, A. Salamat, and R. P. Dias, Synthesis of yttrium superhydride superconductor with a transition temperature up to 262 K by catalytic hydrogenation at high pressures, Phys. Rev. Lett. **126**, 117003 (2021).

[33] Y. Wang, K. Wang, Y. Sun, L. Ma, Y. Wang, B. Zou, G. Liu, M. Zhou, and H. Wang, Synthesis and superconductivity in yttrium superhydrides under high pressure, Chin. Phys. B **31**, 106201 (2022).

[34] L. Ma *et al.*, High-temperature superconducting phase in clathrate calcium hydride CaH_6 up to 215 K at a pressure of 172 GPa, Phys. Rev. Lett. **128**, 167001 (2022).

[35] Z. Li *et al.*, Superconductivity above 200 K discovered in superhydrides of calcium, Nat. Commun. **13**, 2863 (2022).

[36] I. A. Troyan *et al.*, Anomalous high-temperature superconductivity in YH_6, Adv. Mater. **33**, 2006832 (2021).

[37] W. Chen, D. V. Semenok, X. Huang, H. Shu, X. Li, D. Duan, T. Cui, and A. R. Oganov, High-temperature superconducting phases in cerium superhydride with a T_c up to 115 K below a pressure of 1 megabar, Phys. Rev. Lett. **127**, 117001 (2021).

[38] D. V. Semenok *et al.*, Superconductivity at 253 K in lanthanum–yttrium ternary hydrides, Mater. Today **48**, 18 (2021).

[39] W. Chen, X. Huang, D. V. Semenok, S. Chen, K. Zhang, A. R. Oganov, and T. Cui, Nat Commun **14**, 2660 (2023).

[40] J. K. Bi *et al.*, Giant enhancement of superconducting critical temperature in substitutional alloy (La,Ce)H_9, Nat. Commun. **13**, 5952 (2022).

[41] M. Shao, W. Chen, K. Zhang, X. Huang, and T. Cui, High-pressure synthesis of superconducting clathratelike YH_4, Phys. Rev. B **104**, 174509 (2021).

[42] D. Y. Kim, R. H. Scheicher, and R. Ahuja, Predicted high-temperature superconducting state in the hydrogen-dense transition-metal hydride YH_3 at 40 K and 17.7 GPa, Phys. Rev. Lett. **103**, 077002 (2009).

[43] X. Huang *et al.*, High-temperature superconductivity in sulfur hydride evidenced by alternating-current magnetic susceptibility, Natl. Sci. Rev. **6**, 713 (2019).

[44] D. Sun *et al.*, High-temperature superconductivity on the verge of a structural instability in lanthanum superhydride, Nat. Commun. **12**, 6863 (2021).

[45] A. M. Shipley, M. J. Hutcheon, R. J. Needs, and C. J. Pickard, High-throughput discovery of high-temperature conventional superconductors, Phys. Rev. B **104**, 054501 (2021).

[46] C. J. Pickard and R. J. Needs, High-pressure phases of silane, Phys. Rev. Lett. **97**, 045504 (2006).

[47] C. J. Pickard and R. J. Needs, *Ab initio* random structure searching, J. Phys.: Condens. Matter **23**, 053201 (2011).

[48] S. J. Clark, M. D. Segall, C. J. Pickard, P. J. Hasnip, M. J. Probert, K. Refson, and M. C. Payne, First principles methods using CASTEP, Z. Kristallogr. **220**, 567 (2005).

[49] J. P. Perdew, K. Burke, and M. Ernzerhof, Generalized gradient approximation made simple, Phys. Rev. Lett. **77**, 3865 (1996).

[50] G. Kresse and J. Furthmuller, Efficient iterative schemes for *ab initio* total-energy calculations using a plane-wave basis set, Phys. Rev. B **54**, 11169 (1996).

[51] D. J. Chadi, Special points for Brillouin-zone integrations, Phys. Rev. B **16**, 1746 (1977).

[52] G. Kresse and D. Joubert, From ultrasoft pseudopotentials to the projector augmented-wave method, Phys. Rev. B **59**, 1758 (1999).

[53] B. H. Toby, EXPGUI, a graphical user interface for GSAS, J. Appl. Crystallogr. **34**, 210 (2001).

[54] P. Giannozzi *et al.*, QUANTUM ESPRESSO: A modular and open-source software project for quantum simulations of materials, J. Phys.: Condens. Matter **21**, 395502 (2009).

[55] W. L. McMillan, Transition temperature of strong-coupled superconductors, Phys. Rev. **167**, 331 (1968).

[56] P. B. Allen and R. C. Dynes, Transition temperature of strong-coupled superconductors reanalyzed, Phys. Rev. B **12**, 905 (1975).

[57] G. M. Eliashberg, Interactions between electrons and lattice vibrations in a superconductor, Sov Phys JETP **11**, 696 (1960).

[58] See Supplemental Material at http://link.aps.org/supplemental/10.1103/PhysRevB.108.174507 for additional data for the phonon dispersion curves, lattice parameters, Bader charge analysis, electron-phonon coupling parameter, and more.

[59] D. Zhou, D. V. Semenok, D. Duan, H. Xie, W. Chen, X. Huang, X. Li, B. Liu, A. R. Oganov, T. Cui *et al.*, Superconducting praseodymium superhydrides, Sci. Adv. **6**, eaax6849 (2020).